Experiments in Fluids (2022) 63:183
https://doi.org/10.1007/s00348-022-03532-4

RESEARCH ARTICLE

Influence of geometrical parameters on the hysteresis of flutter onset in confined configurations

Girish K. Jankee[1,2] · **Bharathram Ganapathisubramani**[1,2]

Received: 25 June 2022 / Revised: 29 September 2022 / Accepted: 2 November 2022

Abstract

The interaction between a flow and a flexible structure can provide fascinating insight into the vortex shedding phenomenon and any propagation and mixing characteristics, which relate to a plethora of applications such as heat transfer, snoring, musical instruments, or propulsion mechanisms. In this investigation, the influence of confinement on the flapping behaviour of a flexible flag is explored. In particular, hysteresis, one of the least understood aspects of flapping flags, and its sensitivity on both the flexural rigidity of the flag and the confinement ratio is addressed. For the same test-section dimensions and flag material, variations in the flag thickness and flag length enable a range of mass ratios (M^*) and confinement ratios (C^*) to be studied. Pressure measurements and high-speed imaging allow quantification of the hysteretic behaviour. The results demonstrate that although confinement ratio does not contribute to the existence of hysteresis, the relation between the critical reduced velocities and the mass ratio is sensitive to the degree of confinement.

Graphical abstract

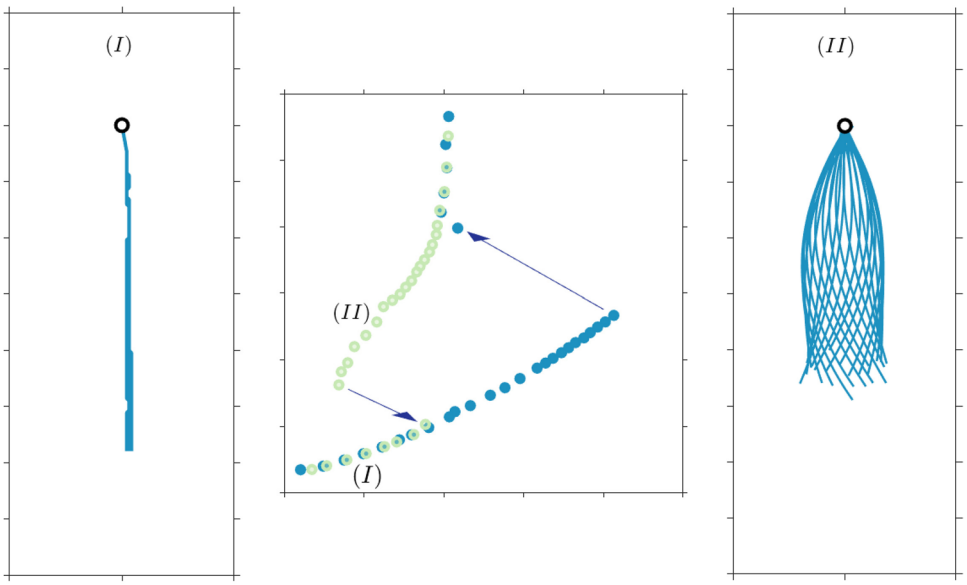

1 Introduction

One of the fundamental enigmas in fluid–structure interactions is associated with the flapping motion of a flag in the presence of an incoming flow. Such a topic has been subjected to intense scrutiny due to its relevance in various

✉ Girish K. Jankee
girish.k.jankee@ntnu.no

Extended author information available on the last page of the article

Published online: 16 November 2022

applications (Shoele and Mittal 2016b). Multiple studies have investigated the fluttering response under a range of varying operating conditions which include but is not limited to confinement, incoming flow properties or structural properties of the flag (Shelley and Zhang 2011). During the interaction of a flag with a crossflow, Yu et al. (2019) categorised the onset of flapping through three different mechanisms. Flapping can be induced through an instability such as the vortex shedding mechanism or through self-excited vibrations. The latter include a positive feedback process between the inertial and elastic forces of the flag and the fluidic forces, which results in increasing aerodynamic loads on the flag and larger amplitudes of motion. Finally, upstream fluctuations in the incoming flow and pressure also represent a source of extraneously induced excitation.

Additionally, Connell and Yue (2007) defined three modes of oscillation (fixed point stability, limit cycle flapping and chaotic flapping) based on the largest Lyapunov exponent (λ) of the time-series of the trailing edge amplitude. In fixed-point stability ($\lambda < 0$), the flag has minimal deflection and is time independent. In the limit cycle flapping regime ($\lambda = 0$), a dominant flapping frequency emerges and any variation in the incoming flow speed has a tendency to alter this dominant frequency. Beyond these operating conditions, the flag motion becomes chaotic ($\lambda > 0$). Although the various possible modes adopted by a flapping flag illustrate the complex physics governing its motion, assumptions can be made to simplify the problem. In this paper, we consider the flag to be a thin membrane immersed in a fluid, fixed at the leading edge and free at the trailing edge. This configuration thus mirrors the salient features of a two-dimensional problem such as dynamical effects of the flow over the membrane, vorticity generation, vortex shedding, structural inertia and restoration forces (Connell and Yue 2007). The properties of the flag and fluid can then be characterised using non-dimensional parameters, which subsequently enable fitting comparison with similar numerical, analytical or experimental studies. Relevant fluidic parameters are the freestream velocity (U_∞), kinematic viscosity (ν) and fluid density (ρ_f) while structural properties of the flag are the Young's modulus (E), the flag length (l), the flag height (h), the thickness of the flag (t) and the flag's material density (ρ_s). Following Eloy et al. (2008) and Gallegos (2017), these variables can be coupled to form the following important non-dimensional parameters:

$$M^* = \frac{\rho_f l}{\rho_s t}. \tag{1}$$

M^* represents the mass ratio, a description of the added mass of the fluid and the mass of the flag.

$$U^* = U_\infty l \sqrt{\frac{\rho_s t}{D}}, \tag{2}$$

where D is the flag bending rigidity, given by:

$$D = \frac{Et^3}{12(1-\nu_s^2)}. \tag{3}$$

U^* represents the reduced velocity and is the ratio between the natural period of the flag and the characteristic time of the fluid passing over it. ν_s is the flag Poisson's ratio. Based on this choice of non-dimensional numbers, the aspect ratio of the flag is $H^* = h/l$ and the channel confinement ratio is defined as $C^* = l/W$, where W is the width of the channel.

1.1 Origin of hysteresis

A flag exposed to an incoming flow is initially in the fixed-point stability regime. As the freestream velocity increases, a critical point is reached where the fluctuations along the oscillation direction of the flag become orders of magnitude higher and a periodic pattern is discernible from the flag's motion. The critical velocity is defined as the velocity at which the flag starts to flap in a Reynolds number (Re) increasing flow, U_i^*, or stops to flap in a Reynolds number decreasing flow, U_d^* (Gallegos and Sharma 2019). Experiments have demonstrated that these critical velocities can be largely different, thus highlighting that under the same flow conditions, a flag can adopt more than one stable regime (Ait Abderrahmane et al. 2011). Such a difference in critical velocity results in a bistability behaviour (hysteresis) which is believed to be primarily influenced by boundary conditions and which can be interpreted as a hysteresis loop with width η:

$$\eta = \frac{U_i^* - U_d^*}{U_i^*}. \tag{4}$$

Attempts to quantify the region over which the bistability behaviour transpires (hysteresis loop) have been made using experiments, numerical simulations and theoretical models (Table 1). A general trend is the under-prediction of the loop width by numerical and theoretical models ($0.1 - 4.5$ %) in comparison to experiments ($15 - 65$ %). Such discrepancy has been attributed to blockage effects, nonlinearity, undesired planeity defects, viscosity and structural damping effects (Tang and Païdoussis 2007; Alben 2008; Eloy et al. 2008). Further, Eloy et al. (2008) argued that the 2D limit of theoretical models cannot be achieved experimentally due to the hysteresis phenomenon and thus 3D effects are inherent in the flutter of large aspect ratio flags, resulting in higher loop width values.

Table 1 Reported range of hysteresis loop width from literature based on theoretical, numerical and experimental studies

Study	Type	η (%)
Zhang et al. (2000)	Experimental	> 40
Watanabe et al. (2002)	Experimental	> 26
Tang and Païdoussis (2007)	Numerical	1 – 4.5
Alben (2008)	Numerical	1 – 3.4
Michelin et al. (2008)	Numerical	2.5 – 4.5
Eloy et al. (2008)	Experimental	> 20
Eloy et al. (2012)	Theoretical/experimental	0.1 – 12.8
Lee et al. (2014)	Numerical	20 – 65
Gallegos and Sharma (2019)	Experimental	15 – 48

The extent over which hysteresis is observed depends on various parameters (Yadykin et al. 2001; Tang et al. 2003; Lemaitre et al. 2005; Eloy et al. 2008; Lee et al. 2014). This study will focus on the confinement effects on hysteresis of flags. Specifically, we will focus on the confinement in the direction orthogonal to the flag plane, due to the separation distance between the walls and the flag's surface. Gallegos and Sharma (2019) studied the influence of this type of confinement on flag flapping dynamics. It was found that confinement in this direction strongly influences the flag dynamics and wake characteristics. Narrower channels restrict the amplitude of the flag oscillations, cause earlier decay of shed vortices and lead to lower turbulence levels inside the channel. The results also showed that confinement and blockage may contribute to hysteresis. However, the experimental data set was not deemed exhaustive enough to provide any direct correlation between hysteresis and the degree of confinement.

In this study, we vary the length of the flag to assess and quantify the sensitivity of hysteresis to the confinement ratio ($C^* = l/W$). We also vary the thickness of the flag and this allows us to examine the influence of mass ratio (M^*) for fixed values of C^*. Varying C^* by changing the flag length also affects the aspect ratio of the flag ($H^* = h/l$). Unfortunately, we are unable to decouple these two parameters within our measurements. However, we did minimise the gap between the flag edges and the spanwise walls as suggested by previous studies to try and achieve two-dimensional flapping and potentially limit the influence of H^*. Overall, these measurements not only allow the validation of existing correlations reported for hysteresis values but also enable new links to be established between the critical reduced velocities and the above-mentioned variables.

2 Experimental setup

A small scale blow-down wind tunnel facility was used for this study. The test-section has a height (H), of 69.7 mm, width (W) of 19.4 mm and a length of 830 mm (Fig. 1). A single inlet 24 V DC fan from ebm-papst Mulfingen GmbH was chosen, capable of delivering a flow rate of up to 225 m^3/h. The experiment targets a velocity range between 1 and 20 m/s, which results in a test-section height-based Reynolds number range between 3300 and 67000 (Eq. 5).

$$Re_H = \frac{U_\infty H}{\nu}, \tag{5}$$

where H is the height of the test-section and ν is the kinematic viscosity of air which has a corresponding value of 1.48 x 10^{-5} m^2/s at conditions of standard temperature and pressure. Part of the test-section is made from acrylic to allow optical access for high-speed imaging and has a removable roof for ease of accessibility and installation of the flag. The flag is connected to a mast made of a carbon fibre rod with a diameter of 1 mm. The flag mast is located at a distance of 40 mm from the onset of the test-section and is secured through a system of collar shafts and set screws found on the outer walls of the removable roof and floor of the test-section. The wind tunnel is positioned vertically, such that the effect of gravity naturally brings the flag to a stable position prior to having a non-zero velocity in the test-section. This avoids the introduction of any bias to the initial angle of attack of the flag, which can result in erroneous critical velocity values, as demonstrated by planeity defects in Eloy et al. (2008). Moreover, all flags extend from wall-to-wall along the height with minimal gap (0.1 mm) at either end to allow free motion of the flag and yet maintain predominantly two-dimensional flow and reduce the potential influence of aspect-ratio of the flag.

Pressure measurements were performed using two Furness controls FC0510 micrometers. Three static probes (P_1, P_2 and P_3), each with a 0.5 mm diameter were placed flushed with the walls and used to measure the differential pressure across the contraction, ΔP_1, as well as the pressure difference across the test-section, ΔP_2 (Fig. 1b). Each pressure measurement was carried out for 30 s at a sampling rate of 15 kHz. The uncertainty in the pressure measurements is based on a standard uncertainty multiplied by a coverage factor of 2 that provides a level of confidence of approximately 95 %. For the range of pressure recorded, the estimated uncertainty in the pressure data is ± 0.03 Pa. A high-speed imaging system was also erected to record the motion of the flag for selected cases. An ultrahigh-speed Photron Fastcam SA1.1 camera, fitted with a 200 mm focal length lens, was used to acquire footage of the flag. Two class 2 green lasers were aligned from either side of the test-section

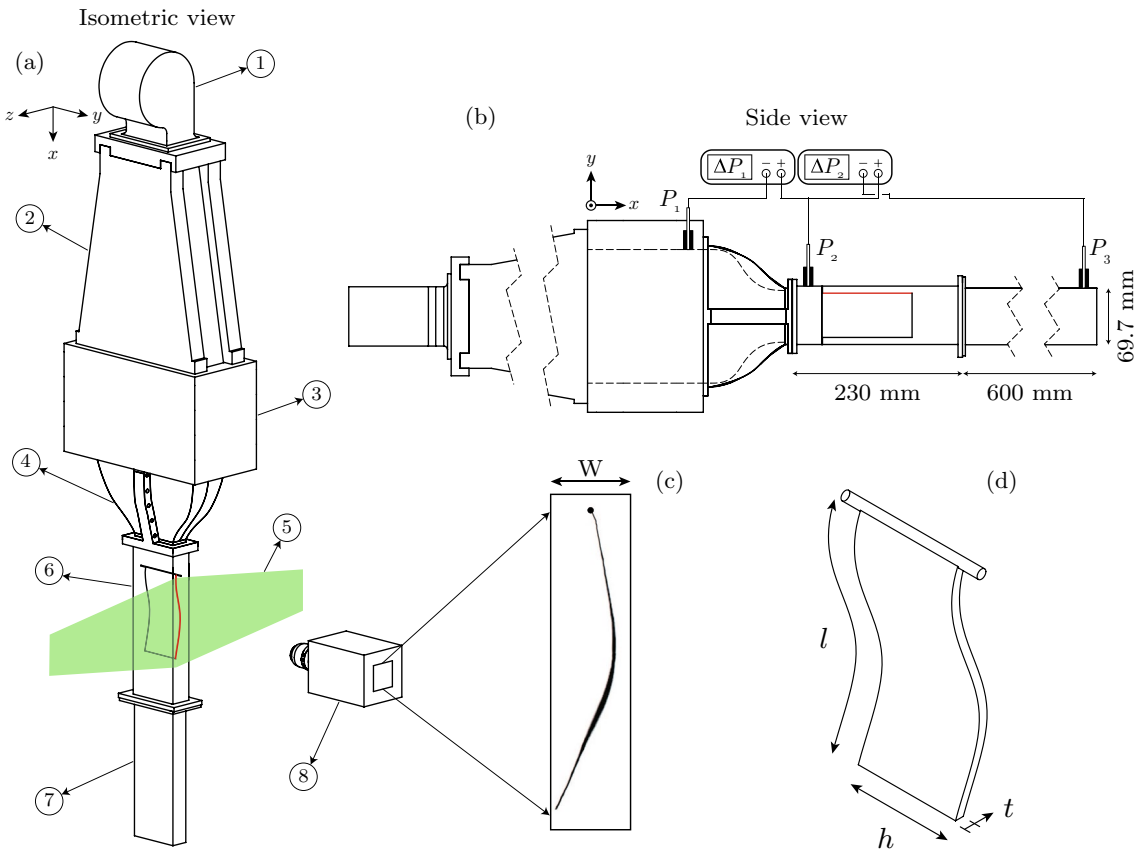

Fig. 1 Schematic of the test facility (not to scale). **a** Isometric view of the blown-down wind tunnel consisting of: 1. Single inlet DC fan, 2. Diffuser, 3. Plenum with flow conditioning, 4. Contraction, 5. Laser sheet, 6. Flag, 7. Test-section and 8. Ultrahigh-speed Photron Fastcam camera. **b** Side view of the facility. P_1, P_2 and P_3 represent the static pressure probes in the plenum, start of test-section and end of test-section, respectively. **c** Example of a snapshot of the flag position from high speed imaging. **d** Geometrical parameters of the flag and their corresponding symbols

and the resulting sheet was aimed at the edge of the flag along the streamwise direction. Images were recorded at a rate of 3600 H*z*, sufficient to meet Nyquist criterion based on the dominant frequencies observed by Gallegos and Sharma (2019). The duration of the acquisition was limited to 6 s*econds* to avoid exceeding the internal memory cache of the camera.

2.1 Test cases

Mylar (*PMX749 industrial polyester*) was selected to manufacture the flag based on its robust properties, e.g., it is durable and has excellent thermal and dimensional stability. The Mylar used has a Young's modulus value, E, of 5.171 x 10^9 Pa and a Poisson's ratio, ν_s, of 0.38. Flag thicknesses ranging from 36 to 175 µm and flag lengths ranging from 19.4 to 77.6 mm, which result in a confinement ratio between 1 and 4, are considered in this parametric study. The flag height is maintained at 69.5 mm, resulting in a flag aspect ratio range between 0.90 and 3.58 (Table 2).

3 Results and discussion

3.1 Critical velocity determination

The critical velocities U_i and U_d are computed from measurements of the pressure difference across the contraction (ΔP_1) based on the abrupt change in differential pressure across the test-section (ΔP_2) when the flag starts or stops to flap. Figure 2 illustrates this procedure. In the absence of hysteresis or if flapping is not induced (Fig. 2a), the same differential pressure measurements are achieved in both the Re-increasing or Re-decreasing part of the cycle. Conversely, Fig. 2(b) shows an example where the bistable condition of a flag can be observed (*Case* 12). In this case, the flag is initially in the fixed point stability regime up to a flow velocity of 12.2 m/s. This stage corresponds to the first critical point (U_i), at which the flag starts to flap and is discernible by the abrupt change in pressure across the test-section. Interestingly, the flapping motion of the flag also appears to be accompanied by a blockage effect

Table 2 Table displaying detailed parameters of the test cases. Combinations of flag lengths, l and flag thicknesses,t, result in 30 test cases. U_i is the critical velocity at which the flag starts to flap, U_d is the critical velocity at which the flag stops to flap and η is the hysteresis loop width

Case #	C^*	H^*	l (mm)	t (μm)	M^*	U_i (m/s)	U_d (m/s)	η (%)
1	1	3.58	19.4	175	0.098	–	–	–
2	1.5	2.39	29.1	175	0.147	-	-	-
3	2	1.79	38.8	175	0.195	–	–	–
4	3	1.19	58.2	175	0.293	13.73	9.02	34.3
5	4	0.90	77.6	175	0.391	7.30	4.94	32.4
6	1	3.58	19.4	125	0.137	–	–	–
7	1.5	2.39	29.1	125	0.205	–	–	–
8	2	1.79	38.8	125	0.274	–	–	–
9	3	1.19	58.2	125	0.410	11.73	3.62	69.1
10	4	0.90	77.6	125	0.547	7.95	4.41	44.5
11	1	3.58	19.4	100	0.171	–	–	–
12	1.5	2.39	29.1	100	0.257	12.25	5.37	56.2
13	2	1.79	38.8	100	0.342	12.15	6.28	48.3
14	3	1.19	58.2	100	0.513	11.58	3.41	70.6
15	4	0.90	77.6	100	0.684	6.75	3.57	47.1
16	1	3.58	19.4	75	0.228	–	–	–
17	1.5	2.39	29.1	75	0.342	11.60	4.33	62.6
18	2	1.79	38.8	75	0.456	11.81	4.03	65.9
19	3	1.19	58.2	75	0.684	8.31	3.02	63.6
20	4	0.90	77.6	75	0.912	6.56	3.36	48.7
21	1	3.58	19.4	50	0.342	–	–	–
22	1.5	2.39	29.1	50	0.513	8.79	4.88	44.5
23	2	1.79	38.8	50	0.684	8.10	4.05	50.1
24	3	1.19	58.2	50	1.026	6.16	3.83	37.9
25	4	0.90	77.6	50	1.368	6.01	2.77	53.9
26	1	3.58	19.4	36	0.475	–	–	–
27	1.5	2.39	29.1	36	0.712	8.58	2.55	70.3
28	2	1.79	38.8	36	0.950	6.49	3.33	48.6
29	3	1.19	58.2	36	1.425	4.75	3.22	32.1
30	4	0.90	77.6	36	1.900	3.89	3.12	19.6

which results in a pressure drop across the contraction. It can be observed from Fig. 2(b) that the increase in differential pressure across the test-section due to the onset of flapping occurs at a lower derived U_∞ value. Such an effect can be attributed to the limited nature of the blower since any subsequent increase in blower power does not result in higher flow velocity although the pressure drop across the flag intensifies. This is illustrated in Fig. 2(c), where the efficiency of the blower is assessed for *Case 12*. The pressure difference across the contraction in the presence of the flag, ΔP_1, is normalised with the pressure difference across the contraction for an empty test section, $(\Delta P_1)_0$, for the same blower power. This confirms that the pressure drop across the contraction is due to the onset of flapping which results in a lower derived U_∞ value. However, this has no incidence on the specific point corresponding to the onset of flapping. For the Re-decreasing part of the cycle, ΔP_2 reduces with flow velocity but flapping is maintained until the lower limit of the critical velocity (U_d) is reached at 5.3 m/s. At U_d, the flag shifts back to the fixed point stability regime and the flow velocity increases as blockage effects are no longer inherent. This trend is consistent with the findings of Eloy et al. (2012) and Gallegos and Sharma (2019). The values of U_i and U_d for each flag configuration are specified in Table 2.

High speed footage of the flag prior to reaching U_d is analysed in Fig. 3. For *Case*11 (Fig. 3a), the flag remains in the fixed point stability regime throughout due to its low M^*. Figure 3(b–d) confirms the limit cycle flapping regime with the time averaged flag position adopting a bell shape envelope in 3(a). Although not shown here, for $C^* > 1$ at higher velocities, the flapping motion became chaotic since the high amplitude of the trailing edge resulted in the flag hitting the test section walls.

3.2 Hysteresis

Hysteresis is quantified using Eq. 4 and the resulting values are plotted against predefined variables (Fig. 4). The range

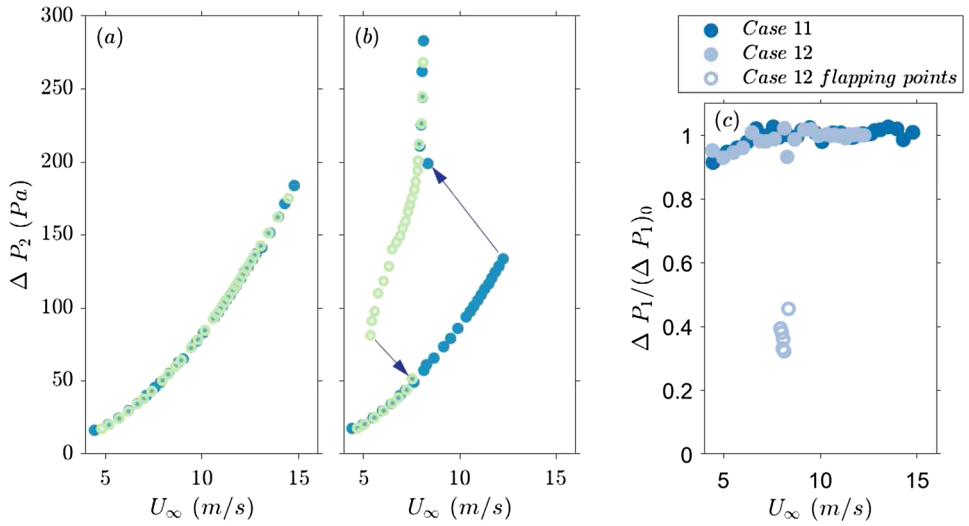

Fig. 2 Variation of the pressure difference across the test-section, ΔP_2, for **a** no hysteresis (*Case* 11) and **b** with hysteresis (*Case* 12). Blue circles correspond to increasing velocity while green circles describe decreasing velocity. **c** Illustration of the blockage effects induced by the flapping motion of the flag for *Case* 12. The pressure difference across the contraction in the presence of the flag, ΔP_1, is normalised with the pressure difference across the contraction for an empty test section, $(\Delta P_1)_0$, for the same blower power and plotted with flow velocity measured at the entrance of the test section

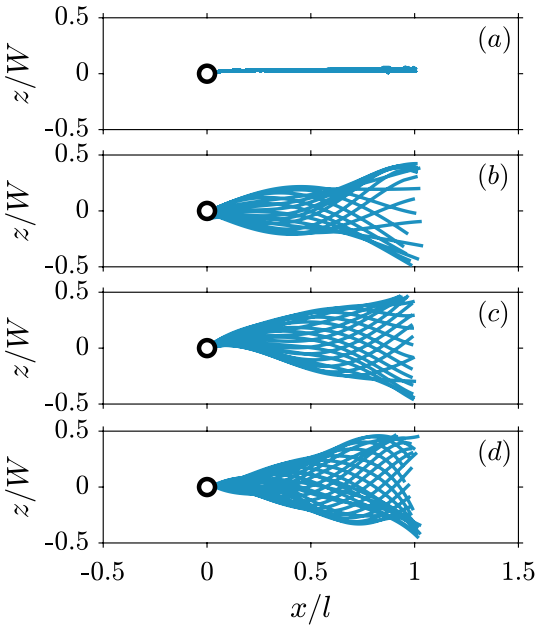

Fig. 3 Snapshots of the flag illustrating the flapping modes observed in the Re-decreasing part of the cycle prior to the flag ceasing to flap for **a** *Case* 11, **b** *Case* 12, **c** *Case* 14, and **d** *Case* 15. The position of the flag is plotted every $\Delta t = 1\ ms$ and is normalised by the corresponding flag length for each case

of hysteresis loop widths obtained in this study ($20-70\%$) is consistent with the results of Lee et al. (2014) and Gallegos and Sharma (2019) but the values of η do not show any conspicuous trend with either confinement ratio or aspect ratio. The contour plots in Fig. 4 demonstrate that peak hysteresis occurs for a specific combination of the flag length and flag thickness. Kim and Lee (2019) attributed large hysteresis values to the large elastic restoration energy of the flag since the hydrodynamic energy should exceed this value for the flag to flap. In fact, a more specific analysis of the critical velocities independently reveals interesting features of how hysteresis varies with confinement or aspect ratio.

Figure 5(a) shows that U_i^* follows a general trend as M^* increases, irrespective of the confinement or aspect ratio. For constant C^* and H^*, an increase in mass ratio can be achieved through a reduction in the flag thickness. From Fig. 5(a), a distinct trend emerges for such cases. U_i^* increases with M^* implying that it becomes easier to initiate flapping for lighter flags since the latter have a lower resistive inertial force, consistent with the observations of Lee et al. (2014) and Gallegos and Sharma (2019). The inability to separate confinement ratio and aspect ratio effects and the small number of cases at a fixed mass ratio limits the analysis of this study.

Figure 5(a) suggests that for the same mass ratio ($M^* = 0.68$), flags necessitate a lower reduced velocity to start flapping as the confinement ratio is increased. Shoele and Mittal (2016a) found that a reduction in the gap between the flag and the walls has a destabilising effect on the dynamics of the system, especially for plates with larger inertia. Higher confinement ratio implies that flags are more prone to shift from a fixed point stability to a limit cycle oscillation regime. Alben (2015) indicated that for heavier flags, higher channel confinement increases the instability while for lighter flags, confinement has minimal influence. When

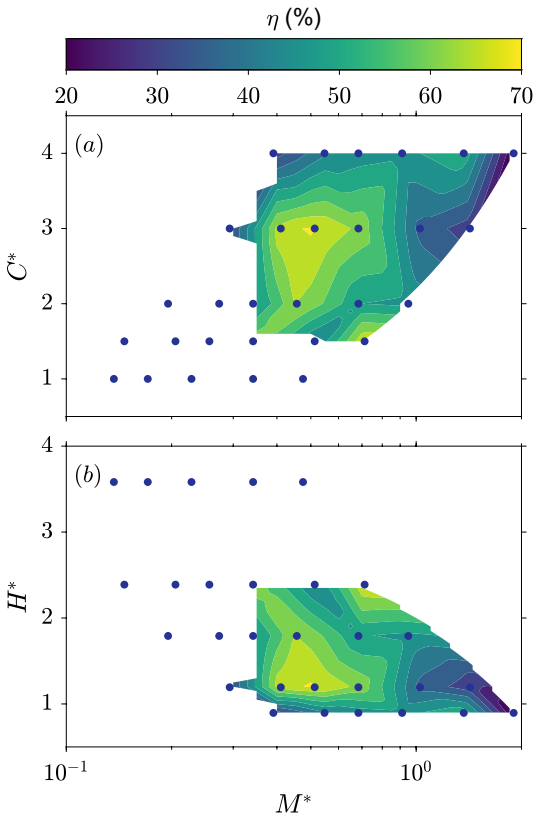

Fig. 4 **a** Contour plot of the hysteresis loop width as the mass ratio and the confinement ratio are varied. **b** Contour plot of the hysteresis loop width as the mass ratio and the flag aspect ratio are varied. It should be noted that the data in subplots (a) and (b) is only interpolated between the measurements points, shown by dark blue circles. Any measurement points in the white space indicate that no hysteresis was captured as the flags did not flap

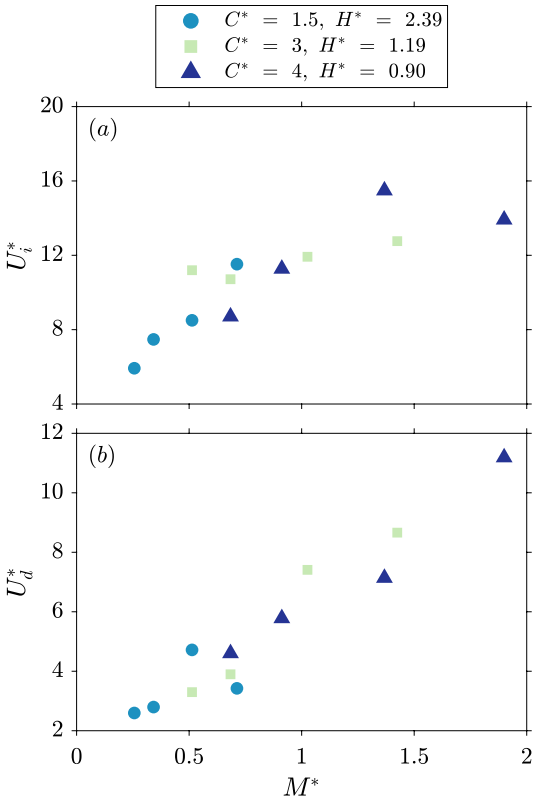

Fig. 5 **a** Plot of the variation of critical velocity for the onset of flapping (U_i^*) against mass ratio for selected confinement and aspect ratios (b) Plot of the variation of critical velocity at which flapping stops (U_d^*) against mass ratio for selected confinement and aspect ratios

M^* is low, i.e. the flag is heavier, confinement effects by the channel walls reduce U_i^*, indicating that for similar inflow speed and mass ratio, increased confinement enhances the instability of a heavy flag. Additionally, higher C^* values also induce ground effect on the flag since the walls are aligned with the flow but orthogonal to the flag's plane of motion. Pressure forces are significantly altered due to the wall, analogous to an airfoil close to the ground. For fixed test-section dimensions, increasing the length of the flag, and C^* in the process, modifies the pressure on either side of the flag. In principle, the pressure is lower due to consequential flow acceleration as opposed to lower C^* cases, similar to the venturi effect, and this results in a lower incoming flow velocity being required for the onset of flapping as the stability of the flag is more likely to get disrupted under such circumstances.

In the Re-decreasing portion of the cycle, the influence of either confinement ratio or aspect ratio on U_d^* is subdued (Fig. 5b). This can be attributed to the local curvature of the flag. In the current study, the flag is constrained at the leading edge while the trailing edge is free to move. This signifies that once the flag achieves limit cycle oscillations, the distance between the channel walls and the flag varies locally along the length of the flag over one flapping cycle. The minimum separation distance occurs at the trailing edge in a mode 2 type oscillation. At this point of the flapping cycle, the shape of the flag is analogous to an airfoil with significant camber, and ground effect results in increased lift which (re)energises the motion of the flag. Hence, the flag remains in the limit cycle oscillation regime for velocities lower than U_i. This justifies the circumscribed influence of the confinement ratio or flag aspect ratio on U_d^*. For a fixed flag length, any minor differences in U_d^* can be attributed to the change in mass ratio, i.e., change in flag thickness and rigidity.

However, it is important to highlight that a more systematic approach is required to differentiate confinement effects from aspect ratio effects. Since the dimensions of the test-section remained constant, the influence of the H^* or C^* on the hysteresis values cannot be decoupled and any change in the flag length resulted in a change in both parameters.

3.3 Critical stability curve and hysteresis

The critical stability curve, a plot of U^* against M^*, depicts the stability of a flag and provides a threshold to distinguish between the stable and unstable modes. Various studies have shown that for a constant value of M^*, an increase in U^* causes the flag to become unstable, with additional significant increase in U^* resulting in periodic flapping transitioning to chaotic motion (Shoele and Mittal 2016b). For unbounded configurations, measurements by Eloy et al. (2008) and Eloy et al. (2012) showed good agreement with linear stability analysis, especially for low aspect ratio flags where hysteresis is insignificant. Eloy et al. (2012) suggested that higher aspect ratio flags experience a larger degree of hysteresis and hence, linear stability analysis tends to underestimate the critical reduced velocity, U_i^*. The results in Fig. 6(a–e) confirm such observations as the critical reduced velocities measured in this study are superimposed upon analytically determined stability curves for multiple confinement ratios from Shoele and Mittal (2016b). Within the limits of experimental uncertainty, it can be concluded that the reduced critical velocities at which the flag starts to flap, U_i^*, are underestimated by the linear stability curves. This confirms the hypothesis of Eloy et al. (2012) that curvature defects are a possible source of hysteresis. Such defects stiffen the flag but are eradicated once flapping begins. Since it is not feasible to include these defects analytically, these models tend to under predict the critical velocity on the Re-increasing part of the hysteresis cycle, as observed here.

Another feature of the stability curve is the existence of lobes which correspond to the different flapping modes adopted by the flag when in the unstable state. Eloy et al. (2008) found that the global shape of the flag correlates to specific modes when the latter are organised in ascending frequencies. In particular, $M^* < 1.5$ described mode 2 (single neck shape), $1.5 < M^* < 5$ corresponded to mode 3 (double neck shape) and so on. For the range of M^* tested in this study, the measured critical velocities describe the first lobe in the stability curve which relates to mode 2. While the use of separate mathematical formulae (e.g. power laws) could have been adopted to scale the reduced critical velocities U_i^* and U_d^* independently, the present aim is to investigate hysteresis as a global feature. It is thus sensible to collectively consider U_i^* and U_d^* measurements as the region bounded by these points is what effectively constitutes the hysteresis loop.

Figure 7(a) demonstrates that an ellipse represents an appropriate fit for describing the loop based on the residual root mean square (r.m.s) error and the associated measurement uncertainty. The ellipse also represents a logical fit as

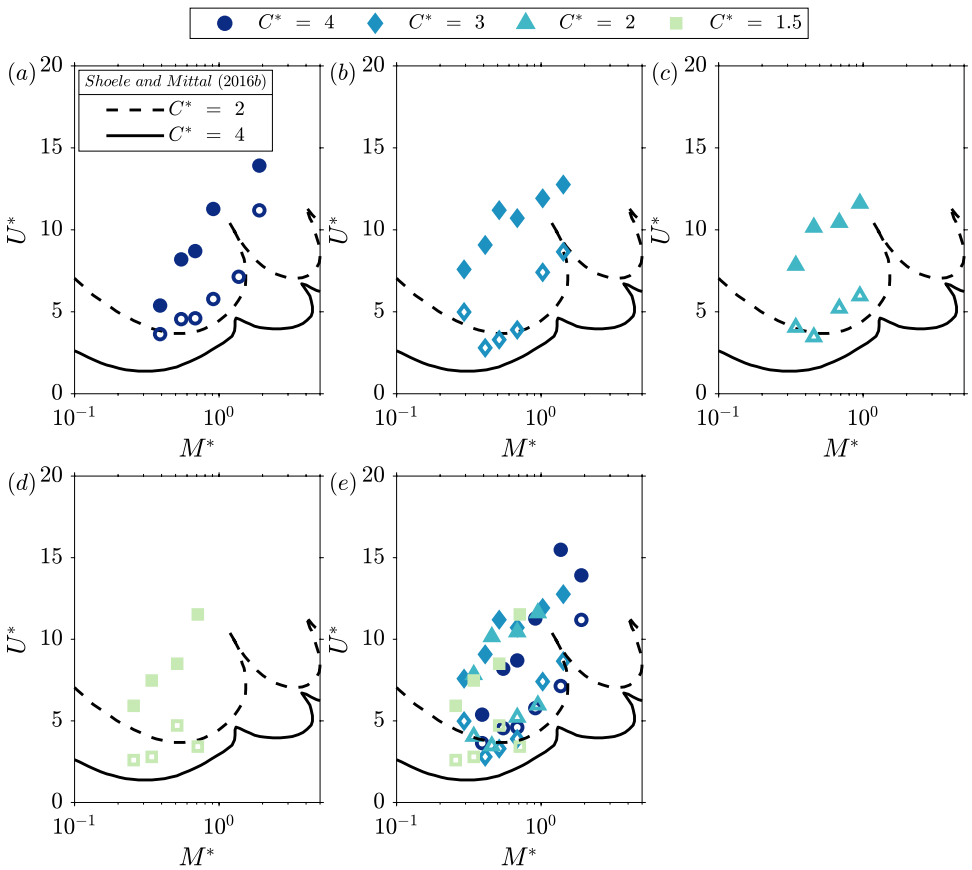

Fig. 6 (a)-(e) Variation of critical velocities U^* with mass ratio M^*. The stability curves for C^* of 2 and 4 from analytical computation by Shoele and Mittal (2016b) are shown as comparison. Filled symbols and open symbols correspond to U_i^* and U_d^*, respectively. **e** Data points from (a)-(d) overlaid on the same figure for multiple C^*

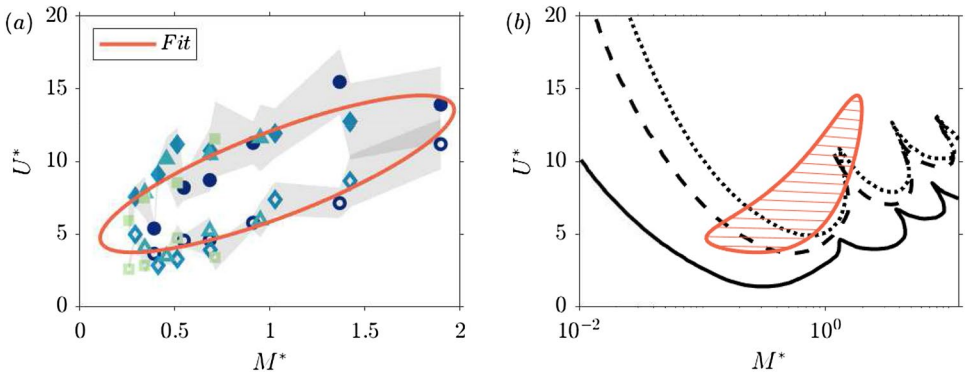

Fig. 7 **a** Elliptical fit from experimental data encompassing the hysteresis region, with the gray band showing the uncertainty in the reduced critical velocity measurements. **b** Correlation between the lobe size in the linear stability curves and the hysteresis loop

its vertices/foci coincides with regions of small hysteresis which occur (i) when the flag is heavy and the confinement ratio is low, i.e., small M^* and small C^*, or (ii) when the flag is light and confinement ratio is high, i.e., high M^* and high C^*. The results indicate that while the existence of hysteresis is hermetic to the confinement ratio, combinations of the latter with flag properties (M^*) dictate the degree of hysteresis observed. This potentially explains why Watanabe et al. (2002) still recorded hysteresis of flapping flags in unconfined space. Finally, we note that the fitting of an ellipse to the data here is a choice made based on observation. Other functional forms may fit the data better, but the current fit appears to do a reasonable job of capturing the trend. Additionally, the elliptical fit determined from Fig. 7(a) is plotted in logarithmic scale on top of stability curves from Shoele and Mittal (2016b) in Fig. 7(b). It can be observed that the fit very conveniently describes the lobe corresponding to mode 2.

4 Conclusion

In summary, an experimental investigation was carried out to explore the influence of hysteresis of flapping flags over a range of differing non-dimensional parameters such as the flag aspect ratio, the mass ratio and the confinement ratio. The results demonstrated that the existence of hysteresis is impervious to confinement but the extent of hysteresis varies through a combination of C^* and M^* and this was attributed to the influence of ground effect. Further, the limitations of linear stability analysis were confirmed as the experimental values of U_i^* were under predicted. The hysteresis loop was also compared to the lobe size in the linear stability curve and was found to conveniently describe the lobe corresponding to mode 2. Finally, this study provides a thorough perspective on hysteresis and the influence of confinement, with a framework that could be extended to additional regimes of the stability curve.

Acknowledgements G.K.J. and B.G. appreciate the contribution of Alexander Hine in designing and building the test facility as part of his BEng individual project.

Author Contributions B.G. conceptualised the research, G.K.J. commissioned the test facility and performed all experiments, G.K.J. and B.G. analysed the data and wrote the manuscript.

Data availability All the data used to produce the figures in this study are included in Table 2 of the manuscript. Raw data are available from the corresponding author (G.K.J.) upon request.

Declarations

Conflicts of interest The authors report no conflict of interest.

References

Ait Abderrahmane H, Païdoussis MP, Fayed M, Ng HD (2011) Flapping dynamics of a flexible filament. Phys Rev E Stat Nonlinear Soft Matter Phys 84(6):1–8. https://doi.org/10.1103/PhysRevE.84.066604

Alben S (2008) The flapping-flag instability as a nonlinear eigenvalue problem. Phys Fluids. https://doi.org/10.1063/1.4915897

Alben S (2015) Flag flutter in inviscid channel flow. Phys Fluids 27(3):033603. https://doi.org/10.1063/1.4915897

Connell BS, Yue DK (2007) Flapping dynamics of a flag in a uniform stream. 581. https://doi.org/10.1017/S0022112007005307

Eloy C, Lagrange R, Souilliez C, Schouveiler L (2008) Aeroelastic instability of cantilevered flexible plates in uniform flow. J Fluid Mech 611:97–106. https://doi.org/10.1017/S002211200800284X,0804.0774

Eloy C, Kofman N, Schouveiler L (2012) The origin of hysteresis in the flag instability. J Fluid Mech 691:583–593. https://doi.org/10.1017/jfm.2011.494

Gallegos RKB, Sharma RN (2017) Flags as vortex generators for heat transfer enhancement: gaps and challenges. Renew Sustain Energy Rev 76:950–962. https://doi.org/10.1016/j.rser.2017.03.115

Gallegos RKB, Sharma RN (2019) Small flags in rectangular channels: dynamics and mean wake characteristics. Int J Mech Sci 155(February):518–535. https://doi.org/10.1016/j.ijmecsci.2019.02.033

Kim MJ, Lee JH (2019) Flapping dynamics of a flexible flag clamped vertically in a viscous uniform flow. J Mech Sci Technol 33(3):1243–1256. https://doi.org/10.1007/s12206-019-0224-2

Lee JH, Wx Huang, Sung HJ (2014) Flapping dynamics of a flexible flag in a uniform flow flapping dynamics of a flexible flag in a uniform flow. Fluid Dyn Res 46:0–21. https://doi.org/10.1088/0169-5983/46/5/055517

Lemaitre C, Hémon P, de Langre E (2005) Instability of a long ribbon hanging in axial air flow. J Fluids Struct 20(7):913–925. https://doi.org/10.1016/j.jfluidstructs.2005.04.009

Michelin S, Smith SG, Glover BJ (2008) Vortex shedding model of a flapping flag. J Fluid Mech 617:1–10. https://doi.org/10.1017/S0022112008004321

Shelley MJ, Zhang J (2011) Flapping and bending bodies interacting with fluid flows. Ann Rev Fluid Mech 43(1):449–465. https://doi.org/10.1146/annurev-fluid-121108-145456

Shoele K, Mittal R (2016) Energy harvesting by flow-induced flutter in a simple model of an inverted piezoelectric flag. J Fluid Mech 790:582–606. https://doi.org/10.1017/jfm.2016.40

Shoele K, Mittal R (2016) Flutter instability of a thin flexible plate in a channel. J Fluid Mech 786:29–46. https://doi.org/10.1017/jfm.2015.632

Tang D, Yamamoto H, Dowell H (2003) Flutter and limit cycle oscillations of two-dimensional panels in three-dimensional axial flow. J Fluids Struct 17(2):225–242. https://doi.org/10.1016/S0889-9746(02)00121-4

Tang L, Païdoussis MP (2007) On the instability and the post-critical behaviour of two-dimensional cantilevered flexible plates in axial flow. J Sound Vib 305(1–2):97–115. https://doi.org/10.1016/j.jsv.2007.03.042

Watanabe Y, Suzuki S, Sugihara M, Sueoka Y (2002) An experimental study of paper flutter. J Fluids Struct 16(4):529–542. https://doi.org/10.1006/jfls.2001.0435

Yadykin Y, Tenetov V, Levin D (2001) The flow-induced vibration of a flexible strip hanging vertically in a parallel flow Part 1: temporal aeroelastic instability. J Fluids Struct 15(8):1167–1185. https://doi.org/10.1006/jfls.2001.0400

Yu Y, Liu Y, Amandolese X (2019) A review on fluid-induced flag vibrations. Appl Mech Rev 71(1):1–17. https://doi.org/10.1115/1.4042446

Zhang J, Childress S, Libchaber A, Shelley M (2000) Flexible filaments in a flowing soap film as a model for one-dimensional flags in a two-dimensional wind. Nature 408(6814):835–839. https://doi.org/10.1038/35048530

Authors and Affiliations

Girish K. Jankee[1,2] · Bharathram Ganapathisubramani[1,2]

Bharathram Ganapathisubramani
G.Bharath@soton.ac.uk

[1] Department of Energy and Process Engineering, Norwegian University of Science and Technology, N-7491 Trondheim, Norway

[2] Aerodyamics and Flight Mechanics, Faculty of Engineering and Physical Sciences, University of Southampton, Southampton SO17 1BJ, UK